Impacts of g-g-v Constraints Formulations on Online Minimum-Time Vehicle Trajectory Planning ⋆

Mattia Piccinini * **Sebastiano Taddei** *,** **Mattia Piazza** * **Francesco Biral** *

* *Department of Industrial Engineering, University of Trento, 38123 Trento, Italy (e-mail: name.surname@unitn.it).*
** *Department of Electrical and Information Engineering, Politecnico di Bari, 70125 Bari, Italy.*

Abstract: The g-g-v diagram is a popular representation of a vehicle's maximum longitudinal and lateral accelerations, as a function of its speed. Recently, g-g-v diagrams have been used as performance constraints for online minimum-time vehicle trajectory planning with economic nonlinear model predictive control (E-NMPC). However, in the related literature, the modeling accuracy of the g-g-v formulations was often compromised in favor of computational efficiency for online E-NMPC. This paper compares various formulations of the g-g-v constraints, evaluating their accuracy, computational efficiency and impact on the lap times, when applied by an artificial race driver (ARD) to control a sports car model on a circuit. Also, we propose a new g-g-v diagram formulation, based on convex polytopic and non-convex polynomial constraints. Our formulation yields improved modeling accuracy while preserving a low computational burden for online E-NMPC. Finally, we analyze the vehicle trajectories, to understand how ARD achieves lower lap times through an improved knowledge of the maximum performance.

Keywords: Autonomous vehicles, autonomous racing, g-g diagram, minimum-time problem, optimal control, model predictive control, trajectory planning.

1. INTRODUCTION

The g-g and g-g-v diagrams are well-known tools to model the maximum performance of a vehicle (Rice, 1973; Biral and Lot, 2009; Tremlett et al., 2014). Specifically, the g-g diagram is a two-dimensional (2D) plot of the maximum reachable longitudinal and lateral accelerations; the g-g-v is a 3D chart, which extends the g-g by showing the dependency on the vehicle speed (Biniewicz and Pyrz, 2023).

Recently, g-g-v diagrams have been applied as performance constraints for online (*i.e.,* real-time) minimum-time trajectory planning (Pagot et al., 2020; Rowold et al., 2023; Piccinini et al., 2023a,b), based on economic nonlinear model predictive control (E-NMPC) (Faulwasser et al., 2018). Using the g-g-v diagram, which collects various non-linearities like aerodynamic drag and tire force saturation, can help reduce the computational burden of online minimum-time E-NMPC.

The mathematical formulation of the g-g-v constraints for minimum-time E-NMPC can hugely impact the final lap time (Rowold et al., 2023). In the literature, most of the g-g-v formulations were either inaccurate in modeling the real shape of the g-g-v diagram, or their computational complexity was too high for online trajectory planning. The main contributions of this paper are:

- A comparison of different formulations of the g-g-v constraints, in terms of (a) accuracy in modeling the g-g-v diagram, (b) computational efficiency for online minimum-time E-NMPC, and (c) impact on the lap time and trajectories achieved by an artificial race driver, which uses E-NMPC to drive a high-fidelity sports car model.
- A new formulation of the g-g-v constraints, combining convex polytopic and non-convex polynomial constraints. Our approach is shown to be more accurate than other formulations in the literature, while maintaining a low computational cost for E-NMPC.

To assess the lap times achievable with different g-g-v formulations, we integrate them into the E-NMPC planner of the artificial race driver (*ARD*) introduced by Piccinini et al. (2023b), for the control of a sports car model.

1.1 Related Work

Some authors recently combined g-g-v constraints with kinematic or kineto-dynamical vehicle models, for online E-NMPC trajectory planning near a vehicle's performance limits (Betz et al., 2022). Various formulations of the g-g-v constraints were used. For example, Rowold et al. (2023) used *diamond shapes* to model the g-g-v constraints. However, their method underestimated the real g-g-v diagram. Montani et al. (2021), Duhr et al. (2022) and

⋆ This work was supported by the European Union Next-GenerationEU (Piano Nazionale di Ripresa e Resilienza (PNRR) - Missione 4 Componente 1, Investimenti 3.4 e 4.1 - Decreto del Ministero dell'Università e della Ricerca n.351 del 09/04/2022) within the Italian National Ph.D. Program in Autonomous Systems (DAuSy).

Novi et al. (2020) combined elliptic and linear g-g-v constraints; however, Novi et al. (2020) overestimated the actual diagram. Elliptic and super-elliptic constraints were used by Pagot et al. (2020) and Piccinini et al. (2023a,b), but they did not analyze the accuracy of the g-g-v diagram approximation.
Veneri and Massaro (2020), Biniewicz and Pyrz (2023) and Lovato and Massaro (2022) employed polar splines to accurately model the g-g-v diagram on 2D and 3D circuits. However, the computational burden of their technique did not allow online E-NMPC.

Critical Summary To our knowledge, no existing paper thoroughly compared the impact of various g-g-v constraint formulations for online minimum-time trajectory planning with E-NMPC. Moreover, many proposed formulations failed to accurately model the actual g-g-v diagram or lacked computational efficiency for online E-NMPC.

2. SIMULATION FRAMEWORK

2.1 Artificial Race Driver (ARD)

The g-g-v formulations of this paper are compared using the artificial race driver (ARD) framework of Piccinini et al. (2023b), shown in Fig. 1. ARD performs high-level trajectory planning with minimum-time E-NMPC, and uses neural feedforward and feedback controllers for low-level trajectory tracking. The g-g-v constraints of this work are integrated into the E-NMPC trajectory planner (blue block in Fig. 1), while the tracking controllers (gray blocks) are the same as in Piccinini et al. (2023b).

2.2 Trajectory Planning E-NMPC Problem

Let us briefly describe the trajectory planning E-NMPC problem, which incorporates the g-g-v constraints:

$$\min_{\boldsymbol{u}\,\in\,\mathcal{U}} \quad \sum_{j=1}^{n_s} \big(\boldsymbol{x}_j(T) - \boldsymbol{x}_{f_j}\big)^2 + \int_0^T w_T \,\mathrm{d}t \tag{1a}$$

$$\text{s.t.} \quad \begin{cases} \dfrac{\mathrm{d}\boldsymbol{x}(t)}{\mathrm{d}t} = \boldsymbol{\mathcal{F}}(\boldsymbol{x}(t), \boldsymbol{u}(t)), & \text{(1b)} \\ \boldsymbol{\mathcal{B}}(\boldsymbol{x}(0)) = 0, & \text{(1c)} \\ \boldsymbol{\mathcal{C}}(\boldsymbol{x}(t), \boldsymbol{u}(t)) \leq 0 & \text{(1d)} \end{cases}$$

The cost function (1a) minimizes the maneuver time T, with w_T being a tunable weight, and sets soft final conditions for the states $\boldsymbol{x}(T)$. The states $\boldsymbol{x}$ and controls $\boldsymbol{u}$ are subject to the dynamics (1b), which is the kineto-dynamical vehicle model of Piccinini et al. (2023b). Equation (1c) sets the initial conditions for $\boldsymbol{x}$, while the inequalities in (1d) enforce the g-g-v constraints, the track limits, and the control bounds. The reader is referred to Piccinini et al. (2023b) for a more detailed description of the E-NMPC problem.
The problem (1) is reformulated using the curvilinear abscissa ζ of the circuit center-line as the independent variable. The prediction horizon is set to 300 m, with a total number of 350 mesh points. The E-NMPC is solved in real-time with the optimal control solver Pins (Biral et al., 2016). Other recent examples of Pins use for online vehicle trajectory planning can be found in Piccinini et al. (2023b); Pagot et al. (2023).

2.3 Vehicle Model for Simulation (VMS)

To assess the impact of various g-g-v formulations on the lap times, we use ARD for closed-loop planning and control of a vehicle model for simulation (*VMS*). The VMS faithfully reproduces the dynamics of a real high-end sports car, with a top speed beyond 300 km/h. The VMS is a double-track vehicle model with roll axis, and is validated with real test-track telemetry data, collected with a professional driver. Additional details and validation plots can be found in Piccinini et al. (2024). The VMS is used for two purposes:

(1) ARD drives the VMS with *online* E-NMPC, using various g-g-v constraint formulations.
(2) A minimum-lap-time OCP (named *MLT-VMS*) is solved *offline* with the full VMS, to benchmark the lap times achieved by ARD with different g-g-v formulations.

2.4 g-g-v Diagram of the VMS

The g-g-v diagram of the VMS is estimated by combining open-loop (OL) and closed-loop (CL) maneuvers. First, the OL tests proposed by Piccinini et al. (2023a) are carried out with the VMS, to assess the maximum longitudinal/lateral accelerations $\{a_x, a_y\}$, as a function of the longitudinal speed v_x. Fig. 2 shows the resulting points of the g-g-v diagram. Second, the CL iterative scheme of Piccinini et al. (2023b) is applied, using the g-g-v diagram as a constraint for CL trajectory planning with E-NMPC. During this phase, a limitation of the combined steering-braking performance is learned (brown planes in Fig. 2), to exclude the unstable g-g-v regions (Tremlett et al., 2014) and improve the closed-loop lap times.
We remark that our g-g-v diagram estimation method can also be applied to a real car. Other techniques were proposed to obtain the g-g-v diagram of a VMS, *e.g.,* optimal control (Massaro et al., 2024).

3. FORMULATIONS OF THE G-G-V CONSTRAINTS

This section outlines the new and benchmark formulations of the g-g-v constraints for minimum-time E-NMPC.

3.1 Proposed Formulation

We propose the following g-g-v formulation:

$$\begin{cases} \boldsymbol{P}\,[a_y \;\; a_x \;\; v_x]^T \leq \boldsymbol{q} & \text{(2a)} \\ \Phi_1(v_x, a_y) \leq a_x \leq \Phi_2(v_x, a_y) & \text{(2b)} \\ a_x \geq \bar{s}\,(|a_y| - \bar{a}_y) & \text{(2c)} \end{cases}$$

The inequality (2a) is the convex hull of the g-g-v points in Fig. 2, and is a set of n_p polytopic constraints [1] in a_y, a_x and v_x. The resulting polytope is defined by the matrix $\boldsymbol{P} \in \mathbb{R}^{n_p \mathrm{x} 3}$ and the vector $\boldsymbol{q} \in \mathbb{R}^{n_p \mathrm{x} 1}$, which are fitted to the g-g-v points.
In (2b), the nonlinear functions $\Phi_1(\cdot)$ and $\Phi_2(\cdot)$ constrain a_x by modeling the non-convex parts of the g-g-v diagram. Indeed, for race cars and motorcycles, the g-g-v regions where a_x is highest and lowest are typically non-convex

[1] The minimum number n_p of polytopic constraints depends on the shape of a given g-g-v diagram. In our case, $n_p = 263$.

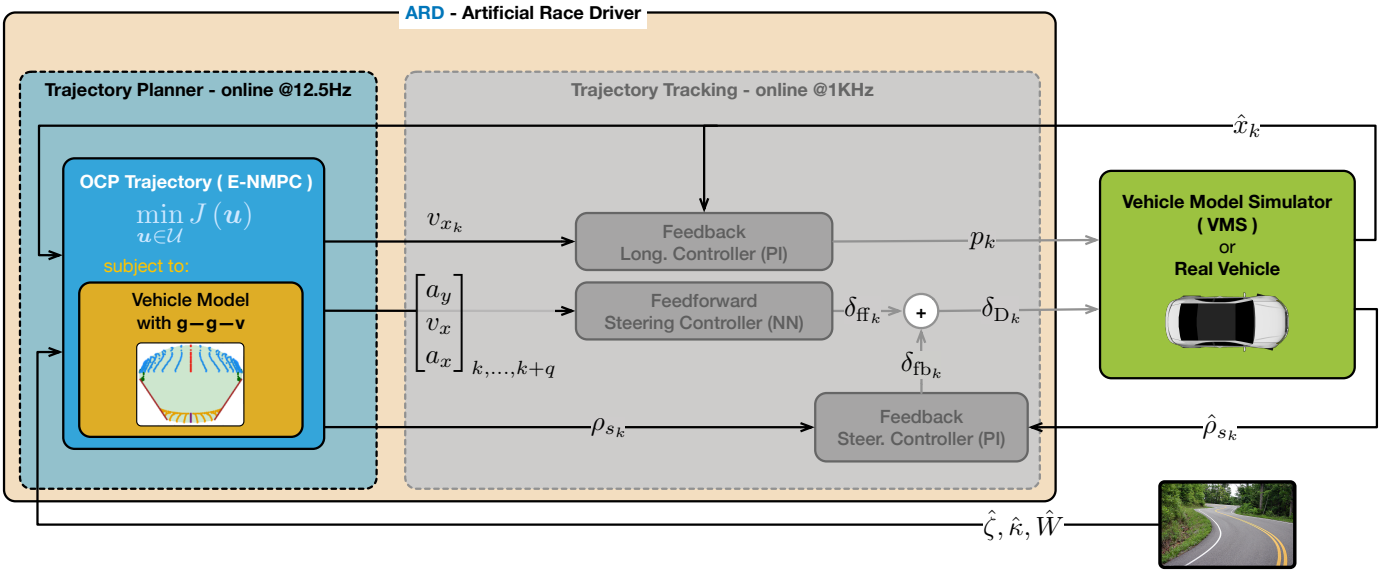

Fig. 1. ARD framework for online minimum-time trajectory planning and control of a vehicle model for simulation (VMS). The g-g-v constraints are integrated into the E-NMPC planner (blue block). The trajectory tracking controllers (gray blocks) are the same of Piccinini et al. (2023b), and they are not in the scope of this paper.

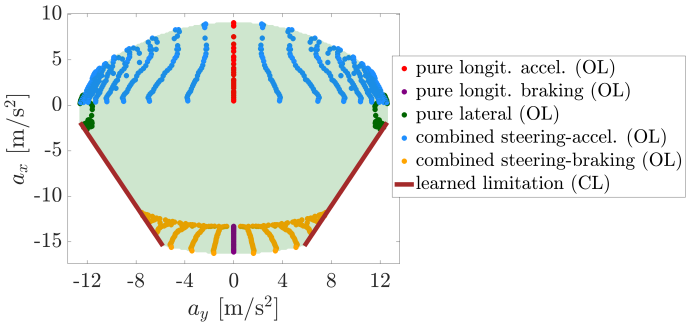

(a) Top view.

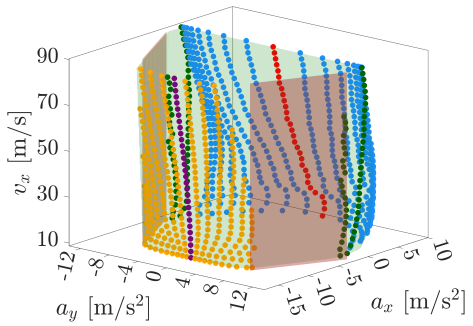

(b) Perspective view.

Fig. 2. g-g-v diagram of the VMS, identified with open-loop (OL) and closed-loop (CL) maneuvers. The green shaded volume represents the reachable accelerations.

(Veneri and Massaro, 2020; Biral and Lot, 2009). We employ a numerically-efficient polynomial formulation for $\Phi_1(\cdot)$ and $\Phi_2(\cdot)$:

$$\begin{cases} \mathrm{w}_{1_i}(v_x) = \sum_{j=0}^{n_v} p_{1_{ji}}\, v_x^j, \quad \mathrm{w}_{2_i}(v_x) = \sum_{j=0}^{n_v} p_{2_{ji}}\, v_x^j & \text{(3a)} \\ \Phi_1(v_x, a_y) = \sum_{i=0}^{n_y} \mathrm{w}_{1_i}(v_x)\, a_y^i & \text{(3b)} \\ \Phi_2(v_x, a_y) = \sum_{i=0}^{n_y} \mathrm{w}_{2_i}(v_x)\, a_y^i & \text{(3c)} \end{cases}$$

where the coefficients $\{p_{1_{ji}}, p_{2_{ji}}\}$, $i = 0, \dots, n_y$, $j = 0, \dots, n_v$, are fitted to the g-g-v points. The polynomial degrees n_v and n_y are chosen to obtain a good fit of the g-g-v points, while keeping a low computational cost for E-NMPC. To model the g-g-v of the sports car in Fig. 2, we set $n_v = 6$ and $n_y = 0$; however, we will show that $n_y > 0$ is typically needed to model the g-g-v of a racing motorcycle.

Finally, the constraint (2c) models the stability limitations of the combined steering-braking performance, as learned from the CL maneuvers of Fig. 2. The parameters $\bar{s}$ and $\bar{a}_y$ in (2c) are fitted to the learned limitations.

Fig. 3 plots the g-g-v constraints, using the model (2).

Generalizability of the Proposed Formulation Our formulation (2) is an extension of Piccinini et al. (2024): the constraints (2b) can now model more generic non-convexities in the g-g-v diagrams of race cars and motorcycles. For example, Fig. 4 shows that our approach can accurately capture the racing motorcycle's g-g diagram of Biral and Lot (2009), in which non-convex regions are present due to the wheelie and stoppie effects. Super-ellipses and diamond shapes (described next) would not be suitable for these types of diagrams.

3.2 Benchmark: g-g-v Formulation with Super-Ellipses

The benchmark g-g-v formulation with super-ellipses is taken from Piccinini et al. (2023b):

$$\begin{cases} \left(a_x - \mathrm{x}_o(v_x)\right)^+ \cdot \left[\left(\frac{|a_y|}{Y(v_x)}\right)^n + \left(\frac{|a_x - \mathrm{x}_o(v_x)|}{X_{\mathrm{M}}(v_x)}\right)^n\right] - \\ \left(a_x - \mathrm{x}_o(v_x)\right)^- \cdot \left[\left(\frac{|a_y|}{Y(v_x)}\right)^n + \left(\frac{|a_x - \mathrm{x}_o(v_x)|}{X_{\mathrm{m}}(v_x)}\right)^n\right] \le 1 \\ \text{(2c)} \end{cases} \tag{4}$$

The first inequality in (4) constrains a_x and a_y with v_x-dependent super-ellipses, whose tunable quantities are the exponent n and the functions $X_{\mathrm{M}}(v_x)$, $X_{\mathrm{m}}(v_x)$, $Y(v_x)$, $\mathrm{x}_o(v_x)$, implemented as polynomials in v_x. $(\cdot)^+$ and $(\cdot)^-$ are smooth functions enabling the use of super-ellipses

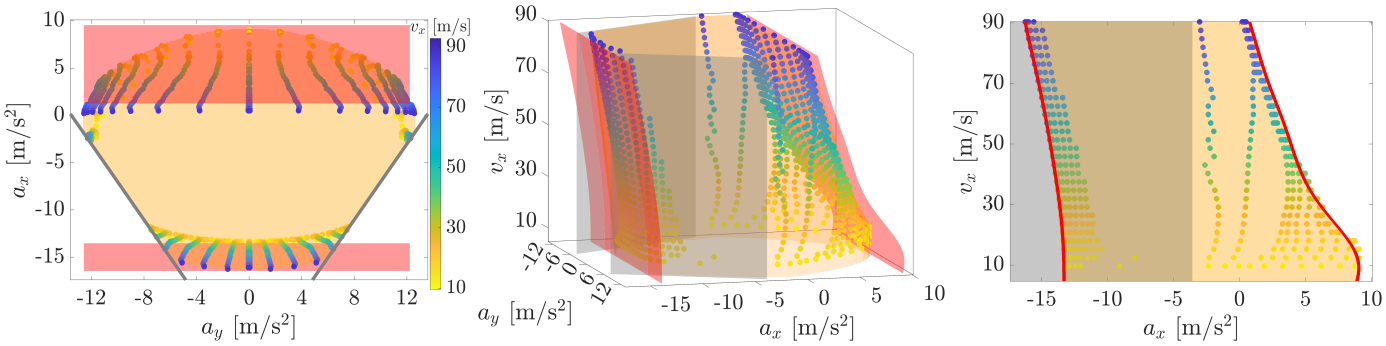

(a) Top view. (b) Perspective view. (c) Side view.

Fig. 3. Modeling the g-g-v diagram of Fig. 2 with our formulation (2): polytopic constraints (2a) (not shown), non-convex constraints (2b) (red curves), stability limitations (2c) (gray planes). The resulting constraint is the orange volume. The colored g-g-v points are the same as in Fig. 2.

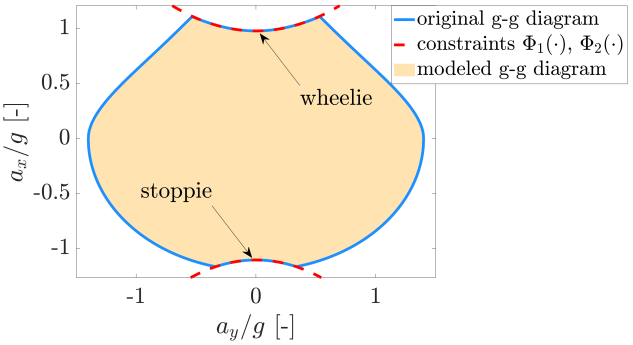

Fig. 4. Applying our formulation (2) to the g-g diagram of the racing motorcycle model in Biral and Lot (2009). The figure shows that our approach can model the non-convex g-g regions due to wheelie and stoppie.

with different sizes, for acceleration and braking. The absolute values in (4) are approximated with a smooth function, defined in Piccinini et al. (2023b). The stability limitation (2c) is added in (4) to constrain the combined steering-braking performance, like in our formulation.

3.3 Benchmark: g-g-v Formulation with Diamond Shapes

The benchmark g-g-v formulation with diamond shapes is taken from Rowold et al. (2023):

$$\begin{cases} a_x \leq a_{x_{\max}}(v_x), \quad |a_y| \leq a_{y_{\max}}(v_x) \\ |a_x| \leq \left|a_{x_{\min}}(v_x)\right| \left[1 - \left(\frac{|a_y|}{a_{y_{\max}}(v_x)}\right)^{n(v_x)}\right]^{\frac{1}{n(v_x)}} \\ \text{(2c)} \end{cases} \tag{5}$$

where the tunable quantities are $a_{x_{\max}}(v_x)$, $a_{y_{\max}}(v_x)$, $a_{x_{\min}}(v_x)$ and the exponent $n(v_x)$, implemented as linear splines in v_x. Note that, in comparison with Rowold et al. (2023), (5) neglects the terms related to a three-dimensional road geometry, since in this work we focus on the g-g-v constraints for a flat road.

3.4 Benchmark: g-g-v Formulation with Polar Splines

The polar spline benchmark formulation of the g-g-v constraint is inspired by Veneri and Massaro (2020):

$$\begin{cases} \rho = \sqrt{a_x^2 + a_y^2}, \quad \alpha = \text{atan2}(a_x, a_y) & \text{(6a)} \\ \rho \leq \rho_{\max}(\alpha, v_x) & \text{(6b)} \end{cases}$$

where ρ is named adherence radius, α is the polar orientation angle, and atan2$(\cdot,\cdot)$ is the two-arguments arctangent. The reachable accelerations are defined by the function $\rho_{\max}(\alpha, v_x)$, which is implemented as a bi-cubic spline.

4. RESULTS

4.1 Approximation of the g-g-v Diagrams

Let us analyze the accuracy of the g-g-v formulations in approximating the g-g-v diagram. The computational efficiency will be discussed in Section 4.2.

Fig. 5 plots the g-g-v diagrams at a low and medium-high vehicle speed. Polar splines provide the best approximation of the g-g-v diagram, since they exactly interpolate the g-g-v points. Super-ellipses are less accurate, especially in the g-g-v regions where $a_x > 0$: they overestimate the g-g-v at low speeds, and underestimate it at high speeds. Indeed, due to their constant [2] exponent n in (4), super-ellipses cannot adequately model the local curvature of the diagram, which changes considerably with v_x. Diamond shapes provide a better approximation of the braking performance, but they overestimate the regions with $a_x > 0$, especially at low speeds. Finally, our formulation provides good accuracy at both low and high speeds, with only a slight overestimation of the braking performance.

4.2 Use of the g-g-v Constraints for Closed-Loop E-NMPC

In this section, we integrate the g-g-v constraints into the E-NMPC problem (1), to compare the computational efficiency of the g-g-v formulations, and their impact on the lap time achieved by our ARD (artificial race driver). As explained in Section 2.1, ARD performs online minimum-time trajectory planning with E-NMPC, and drives the sports car VMS with neural low-level controllers. We test ARD on the Catalunya circuit, a challenging track with low and high-speed corners.

To assess the quality of the lap times achieved *online* by

[2] A better accuracy could be achieved using two different v_x-dependent exponent functions n for the acceleration and braking super-ellipses in (4). However, this would excessively increase the computational complexity, and the E-NMPC could not be solved online with low computational times.

g-g-v formulation	Mean CPU time E-NMPC (*online*)	Std dev CPU time E-NMPC (*online*)	Lap time $T_{\text{MLT}_{\text{vms}}}$ (*offline* MLT-VMS)	Lap time $T_{\text{MLT}_{\text{ard}}}$ (*offline* MLT-ARD)	Lap time T_{ARD} (*online* ARD)
polar splines Veneri and Massaro (2020)	192.7 ms	150.7 ms	114.054 s	114.072 s	ARD cannot operate online
super-ellipses Piccinini et al. (2023b)	15.1 ms	7.6 ms		115.202 s	115.428 s
diamond shapes Rowold et al. (2023)	19.1 ms	10.8 ms		113.025 s	114.841 s
proposed	**28.5** ms	**12.6** ms		114.076 s	**114.348** s

Table 1. Comparing the g-g-v formulations in terms of computational efficiency for E-NMPC; lap time $T_{\text{MLT}_{\text{ard}}}$ of the *offline* MLT-ARD OCP; lap time T_{ARD} achieved by ARD, which drives *online* the VMS with E-NMPC on the Catalunya circuit. Finally, the *offline* MLT-VMS OCP provides our best estimate of the minimum-lap-time, and is used to evaluate the ARD's results.

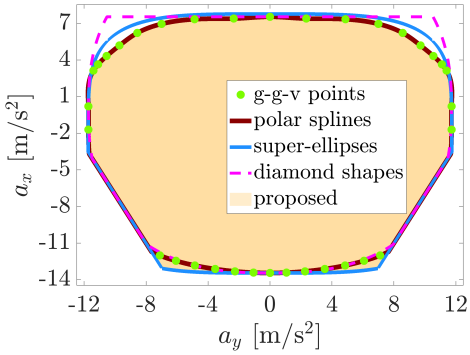

(a) g-g-v diagram at $v_x = 75$ km/h.

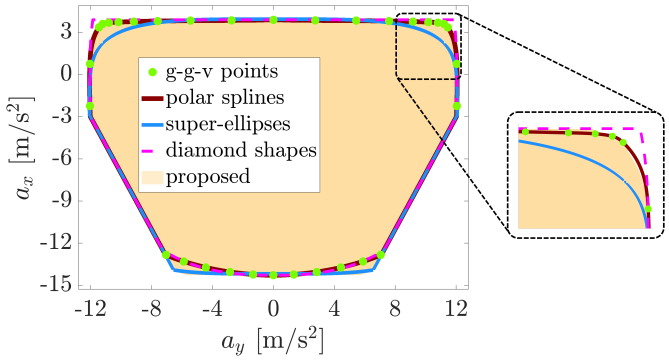

(b) g-g-v diagram at $v_x = 175$ km/h.

Fig. 5. Comparing the g-g-v formulations at $v_x = 75$ km/h (a), $v_x = 175$ km/h (b). Polar splines offer the best approximation but are computationally expensive for online E-NMPC; super-ellipses and diamond shapes are computationally efficient but less accurate. Our method strikes a balance between accuracy and computational efficiency, resulting in the best lap time T_{ARD} (Table 1).

ARD with each g-g-v formulation, we solve *offline* the following OCPs, on a full lap:

- The MLT-VMS OCP of Section 2.3, which is our best estimate of the minimum-lap-time.
- A new OCP, named *MLT-ARD*, with the same formulation and constraints used for E-NMPC (1). The MLT-ARD provides the *theoretical* lap time that a certain g-g-v formulation can achieve, without considering the trajectory feasibility for the VMS.

Lap Times and Computational Efficiency

Table 1 compares the computational efficiency and lap times obtained with each g-g-v formulation. The computational burden is measured by the CPU times (mean and standard deviation) required to solve the E-NMPC problems on one lap of the Catalunya circuit. The E-NMPC problems are re-computed online every 80 ms, on a MacBook Pro laptop with a 2.6 GHz 6-Core Intel i7 processor.

Polar splines: The polar spline approach provides the best modeling accuracy: the MLT-ARD offline solution sets a lap time very close (18 ms) to the MLT-VMS reference. However, polar splines are computationally inefficient for E-NMPC, with a high mean CPU time (192.7 ms) and standard deviation (150.7 ms). Considering our re-planning sample time of 80 ms, polar splines do not allow ARD to operate online. Indeed, Veneri and Massaro (2020) used their polar spline approach only for *offline* trajectory optimization.

Super-ellipses: The formulation with super-ellipses is the most computationally efficient, with the lowest mean CPU time (15.1 ms) and standard deviation (7.6 ms). However, the lap time T_{ARD} is 1.374 s higher than the MLT-VMS benchmark, due to the worse approximation of the g-g-v diagram, which can be noticed in Fig. 5.

Diamond shapes: As discussed in Section 4.1, diamond shapes overestimate the combined steering-acceleration regions of the g-g-v. This leads to a lower *theoretical* lap time $T_{\text{MLT}_{\text{ard}}}$ (1.029 s below the MLT-VMS). However, due to the g-g-v overestimation, the trajectories planned by E-NMPC are locally infeasible for the VMS, and ARD achieves a higher lap time when driving in closed-loop (0.787 s worse than the MLT-VMS). The advantage of diamond shapes is the computational efficiency: the mean CPU time for online E-NMPC is 19.1 ms.

Proposed formulation: Our approach yields the best lap time T_{ARD}, which is only 0.294 s higher than the MLT-VMS benchmark. The mean CPU time is 28.5 ms, which is slightly higher than the diamond shapes formulation, but still allows ARD to operate online with a re-planning sample time of 80 ms. As discussed in Section 4.1, our formulation provides a good approximation of the g-g-v diagram, both at low and high vehicle speeds.
Fig. 6 plots the accelerations achieved online by ARD with

our g-g-v model, and by the MLT-VMS offline solution, on the Catalunya circuit. The figure shows that ARD and the MLT-VMS solution achieve similar maximum accelerations, which confirms that our formulation allows ARD to drive close to the handling limits.

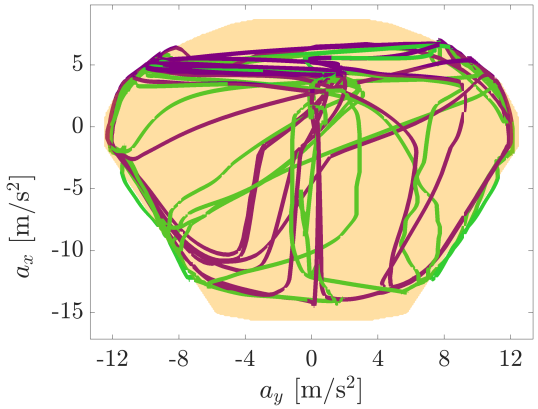

(a) Top view.

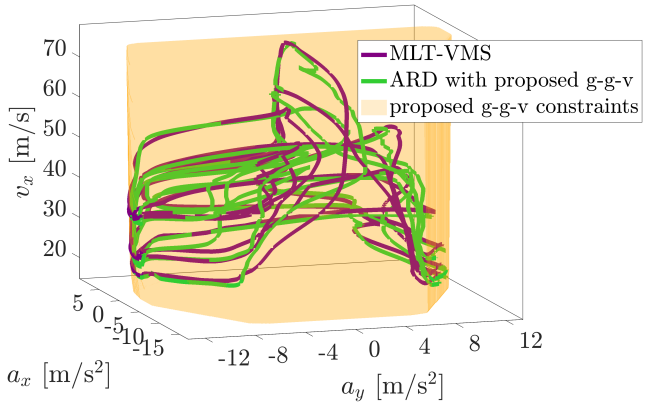

(b) Perspective view.

Fig. 6. g-g-v diagram, Catalunya circuit: comparing the accelerations achieved online by ARD with the proposed g-g-v constraints, and by the benchmark offline MLT-VMS, which uses the full VMS in the OCP.

Analysis of the Vehicle Trajectories

Fig. 7 analyzes the vehicle trajectories, velocity profiles and maneuver times executed by ARD at the corner n.5 of the Catalunya circuit, with the three g-g-v formulations enabling online E-NMPC. In the corner entry (sector A-B), our formulation leads to a similar trajectory and speed as the super-ellipses. Conversely, diamond shapes locally overestimate the vehicle performance (Fig. 5), so ARD carries more speed into the corner. However, the trajectory planned with diamond shapes is locally infeasible: ARD needs to re-plan and execute a wider and slower maneuver (point C), which increases the travel time. In the corner exit (sector C-D), super-ellipses slightly underestimate the combined steering-acceleration performance, while our approach results in a higher local speed, similar path and lower maneuver times.
Considering the whole maneuver A-D, our g-g-v formulation enables ARD to drive faster than super-ellipses (by 0.03 s) and diamond shapes (by 0.11 s), which is not negligible on a sector of only 150 m.

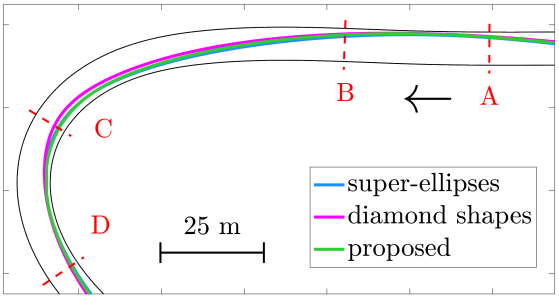

(a)

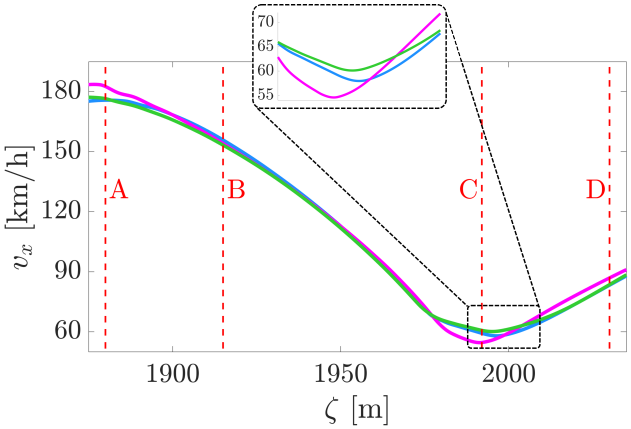

	maneuver time t [s]		
	super-ellipses	diamond-shapes	proposed
A	0.00	0.00	0.00
B	0.75	0.74	0.75
C	3.54	3.63	3.54
D	5.41	5.49	5.38

(b)

Fig. 7. Vehicle trajectories, velocity profiles and maneuver times executed by ARD at the corner n.5 of the Catalunya circuit, with different g-g-v formulations for E-NMPC.

5. CONCLUSIONS

This paper compared existing and new formulations of the g-g-v performance constraints for online minimum-time trajectory planning with E-NMPC. We evaluated the literature techniques that used polar splines, super-ellipses and diamond shapes. Also, a new g-g-v formulation was introduced, based on polytopic and polynomial constraints. The g-g-v constraints were integrated into the E-NMPC problem of our ARD agent, which was applied to drive a high-fidelity VMS on a test circuit.
The results indicate that our approach provides a better approximation of the g-g-v diagram, and it enables online E-NMPC with low computational times. By analyzing the vehicle trajectories, we discussed how our method allowed ARD to be faster in many corners. As a result, ARD achieved a lap time very close to the MLT-VMS OCP solution, which was our best lap time estimate.
Finally, our modeling technique showed good generalizability when applied to a racing motorcycle's g-g diagram, providing an accurate approximation of its non-convex regions.

REFERENCES

Betz, J., Zheng, H., Liniger, A., Rosolia, U., Karle, P., Behl, M., Krovi, V., and Mangharam, R. (2022). Autonomous vehicles on the edge: A survey on autonomous vehicle racing. *IEEE Open Journal of Intelligent Transportation Systems*, 3, 458–488. doi: 10.1109/OJITS.2022.3181510.

Biniewicz, J. and Pyrz, M. (2023). A quasi-steady-state minimum lap time simulation of race motorcycles using experimental data. *Vehicle System Dynamics*, 0(0), 1–23. doi:10.1080/00423114.2023.2170256.

Biral, F., Bertolazzi, E., and Bosetti, P. (2016). Notes on numerical methods for solving optimal control problems. *IEEJ Journal of Industry Applications*, 5, 154–166. doi: 10.1541/ieejjia.5.154.

Biral, F. and Lot, R. (2009). An interpretative model of g-g diagrams of racing motorcycle. In *Proceedings of the 3rd ICMEM International Conference on Mechanical Engineering and Mechanics*. Beijing, China.

Duhr, P., Sandeep, A., Cerofolini, A., and Onder, C.H. (2022). Convex performance envelope for minimum lap time energy management of race cars. *IEEE Transactions on Vehicular Technology*, 71(8), 8280–8295. doi: 10.1109/TVT.2022.3172473.

Faulwasser, T., Grüne, L., and Müller, M.A. (2018). *Economic Nonlinear Model Predictive Control*.

Lovato, S. and Massaro, M. (2022). A three-dimensional free-trajectory quasi-steady-state optimal-control method for minimum-lap-time of race vehicles. *Vehicle System Dynamics*, 60(5), 1512–1530. doi: 10.1080/00423114.2021.1878242.

Massaro, M., Lovato, S., and Veneri, M. (2024). An optimal control approach to the computation of g-g diagrams. *Vehicle System Dynamics*, 62(2), 448–462. doi:10.1080/00423114.2023.2178467.

Montani, M., Ronchi, L., Capitani, R., and Annicchiarico, C. (2021). A hierarchical autonomous driver for a racing car: Real-time planning and tracking of the trajectory. *Energies*, 14(19). doi:10.3390/en14196008.

Novi, T., Liniger, A., Capitani, R., and Annicchiarico, C. (2020). Real-time control for at-limit handling driving on a predefined path. *Vehicle System Dynamics*, 58(7), 1007–1036. doi:10.1080/00423114.2019.1605081.

Pagot, E., Piccinini, M., Bertolazzi, E., and Biral, F. (2023). Fast planning and tracking of complex autonomous parking maneuvers with optimal control and pseudo-neural networks. *IEEE Access*, 11, 124163–124180. doi:10.1109/ACCESS.2023.3330431.

Pagot, E., Piccinini, M., and Biral, F. (2020). Real-time optimal control of an autonomous rc car with minimum-time maneuvers and a novel kineto-dynamical model. In *2020 IEEE/RSJ International Conference on Intelligent Robots and Systems (IROS)*, 2390–2396. doi: 10.1109/IROS45743.2020.9340640.

Piccinini, M., Larcher, M., Pagot, E., Piscini, D., Pasquato, L., and Biral, F. (2023a). A predictive neural hierarchical framework for on-line time-optimal motion planning and control of black-box vehicle models. *Vehicle System Dynamics*, 61(1), 83–110. doi:10.1080/00423114.2022.2035776. URL `https://doi.org/10.1080/00423114.2022.2035776`.

Piccinini, M., Taddei, S., Larcher, M., Piazza, M., and Biral, F. (2023b). A physics-driven artificial agent for online time-optimal vehicle motion planning and control. *IEEE Access*, 11, 46344–46372. doi: 10.1109/ACCESS.2023.3274836.

Piccinini, M., Taddei, S., Pagot, E., Bertolazzi, E., and Biral, F. (2024). How optimal is the minimum-time manoeuvre of an artificial race driver? *Vehicle System Dynamics*. Under review.

Rice, R.S. (1973). Measuring car-driver interaction with the g-g diagram. In *1973 International Automotive Engineering Congress and Exposition*, 22. doi: 10.4271/730018.

Rowold, M., Ögretmen, L., Kasolowsky, U., and Lohmann, B. (2023). Online time-optimal trajectory planning on three-dimensional race tracks. In *2023 IEEE Intelligent Vehicles Symposium (IV)*, 1–8. doi: 10.1109/IV55152.2023.10186701.

Tremlett, A., Assadian, F., Purdy, D., Vaughan, N., Moore, A., and Halley, M. (2014). Quasi-steady-state linearisation of the racing vehicle acceleration envelope: a limited slip differential example. *Vehicle System Dynamics*, 52(11), 1416–1442. doi: 10.1080/00423114.2014.943927.

Veneri, M. and Massaro, M. (2020). A free-trajectory quasi-steady-state optimal-control method for minimum lap-time of race vehicles. *Vehicle System Dynamics*, 58(6), 933–954. doi:10.1080/00423114.2019.1608364.